

# **Detonations in Hydrocarbon Fuel Blends**

J.M. Austin and J.E. Shepherd

Graduate Aeronautical Laboratories,  
California Institute of Technology  
Pasadena, California 91125

Explosion Dynamics Laboratory Report FM99-6  
July 10, 2000

Prepared for the Air Force and Advanced Projects Research Inc.,  
under contract F04611-98-C-0046

## Abstract

A study of detonations in high molecular weight hydrocarbon fuels was performed in two GALCIT facilities: the 280 mm gaseous detonation tube (GDT) and a 1180 liter vessel (HYJET) with jet initiation capability.

In the GDT, detonation pressure, wave speed and cell width measurements were made in hexane-oxygen-nitrogen mixtures with and without the addition of lower molecular weight fuels. Stoichiometric mixtures of hexane-oxygen were studied with nitrogen dilution varying from fuel-oxygen to fuel-air. Hexane-air mixtures were investigated with varying fractions of lower molecular weight fuels (hydrogen, acetylene, ethylene, and carbon monoxide). The measured cell width decreased indicating increased sensitivity to detonation with increasing fraction of hydrogen, acetylene, and ethylene, in order of effectiveness. The addition of a small fraction of carbon monoxide produced a small decrease in the cell width, but addition of more than about 75 % (by fuel mass) carbon monoxide resulted in a rapid increase in cell width.

As the oxidation of carbon monoxide is extremely sensitive to the presence of hydrogenous species, cell width measurements were made in carbon monoxide-air mixtures with the addition of hydrogen or hydrocarbons of various H-atom content and structure (acetylene, ethylene, and hexane). A detonation could be initiated in mixtures with very small fraction of hexane (0.07% of the mixture volume). Cell width measurements were compared to calculated ZND reaction zone parameters, including temperature and radical species concentrations. It was determined that for addition of hydrogen, ethylene or hexane, the cell width can be correlated with the product of the peak OH and CO concentrations in the reaction zone. Mixtures containing acetylene also showed the same linear dependence on this parameter, but, for the same peak OH and CO concentration, the cell widths were a factor of two smaller than those of the other mixtures.

A fuel blend representative of thermally decomposed JP-10 was studied at 295 K. This blend consisted of hydrogen, carbon monoxide, methane, acetylene, ethylene, and hexane with varying fractions of oxygen and nitrogen. The cell width for stoichiometric fuel blend-oxygen was found to be an order of magnitude smaller than that for fuel blend-air. The cell width for the fuel blend-air mixture was about half that of hexane-air.

Further experiments were carried out in the HYJET facility. A hydrogen-oxygen-nitrogen jet was used to initiate detonations in vapor phase mixtures

of hexane (at 295 K) and of dodecane (at 380 K) with stoichiometric oxygen. Pressure and wave speed measurements were made. A critical nitrogen dilution limit was determined for each fuel. The critical limit was found to be  $2.5 \leq \beta \leq 3.0$  for hexane, where  $\beta$  is the ratio of nitrogen to oxygen concentration. This corresponds to a  $D/\lambda$  (nozzle diameter/cell width) ratio of 4, which compares well with the value 4.3 previously determined for this driver. The critical nitrogen dilution limit for dodecane was also found to be  $2.5 \leq \beta \leq 3.0$ . No cell width measurements are currently available for dodecane.

An attempt was made to initiate detonation in a dodecane spray. Pressure and velocity measurements were made and clearly show that no detonation could be directly initiated. Different fuel injection systems were tried and the initial temperature of the mixture was varied.

# Contents

<b>I Sensitization of High Molecular Weight Hydrocarbons</b>	<b>1</b>
1 Introduction	1
2 Facility Description	2
3 Cell Width Measurements	5
3.1 C <sub>6</sub> H <sub>14</sub> Mixtures with O <sub>2</sub> -N <sub>2</sub> . . . . .	5
3.2 Sensitization of C <sub>6</sub> H <sub>14</sub> -air . . . . .	9
3.3 Addition of H <sub>2</sub> , C <sub>2</sub> H <sub>2</sub> , C <sub>2</sub> H <sub>4</sub> , and C <sub>6</sub> H <sub>14</sub> to CO-air . . . . .	12
3.4 Decomposed JP-10 Surrogate (HCS) . . . . .	24
<b>II Homogeneous and Heterogeneous Detonations in C<sub>6</sub>H<sub>14</sub> and C<sub>12</sub>H<sub>26</sub></b>	<b>25</b>
4 Introduction	26
5 Facility Description	26
6 Driver Characterization	28
7 Vapor Phase Experiments in Hexane and Dodecane	31
7.1 Hexane . . . . .	31
7.2 Dodecane . . . . .	34
8 Heterogeneous Experiments in Dodecane	35
8.1 Facility Modifications . . . . .	35
8.2 Results . . . . .	37
9 Summary and Conclusions	41
A Tables of experimental conditions and results	47

## List of Figures

1	GALCIT 280 mm diameter gaseous detonation facility. . . . .	2
2	Soot foil for shot 1007: $C_6H_{14}+9CO+14$ Air. Detonation propagated right to left. . . . .	3
3	Pressure traces for shot 1007. . . . .	3
4	Cell width measurements for $N_2$ dilution of $C_6H_{14}-O_2$ mixtures. Experiment parameters are given in Table A . . . . .	6
5	Comparison of cell width measurements for $N_2$ dilution of $CH_4$ , $C_2H_4$ , $C_3H_8$ and $C_6H_{14}-O_2$ mixtures. $C_6H_{14}$ data is the same as that presented in Fig.4 . . . . .	7
6	Comparison of cell width measurements for $N_2$ dilution of $H_2$ , $C_2H_2$ mixtures with $O_2$ . . . . .	8
7	Cell width measurements for $H_2$ addition to $C_6H_{14}$ in air. Experiment conditions are given in Table A. . . . .	9
8	Cell width measurements for $C_2H_2$ addition to $C_6H_{14}$ in air. Experiment conditions are given in Table A. . . . .	10
9	Cell width measurements for $C_2H_4$ addition to $C_6H_{14}$ in air. Experiment conditions are given in Table A. . . . .	10
10	Cell width measurements for CO addition to $C_6H_{14}$ in air. Experiment conditions are given in Table A. . . . .	11
11	Cell width measurements for $N_2$ dilution of stoichiometric CO-5% $H_2-O_2$ . See Table A for experiment conditions. . . . .	12
12	Cell width measurements for hydrogen or hydrocarbon addition to CO-air mixtures. Curves are interpolated from the cell widths of successful detonations. Error bars represent minimum and maximum measured cell widths. The detonation limit denotes a mixture where at least one failure was observed. About three experiments were performed for each mixture that resulted in a failure. Conditions and data are given in Table A . . . . .	14
13	Measured cell width against initial H/CO ratio. Only successful detonations are shown. . . . .	15
14	Mechanism validation for CO- $H_2$ - $O_2$ -Ar mixtures. Shock tube data is for the mixture 0.049% $H_2$ , 1.01% $O_2$ , 3.28% CO, Ar. . . . .	16

15	Mechanism validation for C <sub>6</sub> H <sub>14</sub> -O <sub>2</sub> -Ar mixtures. Circles and dashed lines correspond to data and calculations respectively for mixture A. Squares and solid lines correspond to data and calculations respectively for mixture B. . . . .	17
16	Cell width measurements versus reaction zone thickness in CO-O <sub>2</sub> mixtures with hydrogenous additive at 100 kPa. The reaction zone thickness is defined by a) the location of the maximum temperature gradient or b) by the location of the OH peak. . . . .	19
17	Calculated species mole fractions through the reaction zone in stoichiometric CO-H <sub>2</sub> -air mixtures. H <sub>2</sub> quantities are by fuel mole fraction. . . . .	20
18	Peak OH mole fraction against initial [H]/[CO] ratio. . . . .	21
19	Calculated species mole fractions through the reaction zone in stoichiometric CO-C <sub>6</sub> H <sub>14</sub> -air. Note the differences in scale on the ordinate axis. . . . .	22
20	Correlation of measured cell width against the parameter 1/([OH][CO]). Species concentrations are calculated by a ZND code and evaluated at the OH peak. . . . .	23
21	Cell width measurements for N <sub>2</sub> dilution of a hydrocarbon blend representative of decomposed JP-10. The initial pressure was increased with increasing N <sub>2</sub> dilution. . . . .	25
22	HYJET receiver instrumentation. (Driver vessel not shown.)	27
23	Ionization gauge located in the driver of the HYJET facility. The receiver contained air at 1 atm. . . . .	28
24	Schematic of the ionization gauge circuit, V <sup>+</sup> =12V. . . . .	29
25	Time-of-arrival data from ionization gauges in the driver. . . . .	30
26	Pressure traces recorded along the receiver vessel wall for vapor phase C <sub>6</sub> H <sub>14</sub> -O <sub>2</sub> -N <sub>2</sub> mixtures. On the left, $\beta = 2.25$ (shot 569). The initial pressure was 690 mbar, the initial temperature 298 K. On the right, $\beta = 3.0$ (shot 571). The initial pressure was 844 mbar, the initial temperature 296 K. Note the difference in scale on the ordinate axes. . . . .	31
27	D/ $\lambda$ (nozzle diameter/measured cell width) variation with nitrogen dilution. Initial pressure increased with increasing N <sub>2</sub> dilution. . . . .	32

28	Pressure traces recorded along the receiver vessel wall for vapor phase $C_{12}H_{26}-O_2-N_2$ mixtures. On the left, $\beta = 2.5$ (shot 581). The initial pressure was 738 mbar, the initial temperature 381 K. On the right, $\beta = 3.0$ (shot 579). The initial pressure was 842 mbar, the initial temperature 380 K. Note the difference in scale on the ordinate axes. . . . .	34
29	HYJET facility receiver vessel: two-port injection system configuration. (Driver vessel not shown.) . . . . .	35
30	Pressure traces recorded along the receiver vessel wall and at the end wall for heterogeneous $C_{12}H_{26}-O_2$ mixtures. On the left, (shot 590) the initial temperature was 25 °C and only a decaying shock is observed. On the right, (shot 591) the initial temperature was 65 °C and a detonation is initiated on reflection. The two-port injection system was used in both cases. Note the difference in scale on the ordinate axes. . . . .	38
31	HYJET facility receiver vessel: manifold injection system configuration. (Driver vessel not shown.) . . . . .	39
32	Pressure traces recorded along the receiver vessel wall and at the end wall for heterogeneous $C_{12}H_{26}-O_2$ mixtures. On the left, (shot 594) the initial temperature was 50 °C; on the right, (shot 595) the initial temperature was 65 °C. The manifold injection system was used in both cases. Note the difference in scale on the ordinate axes. . . . .	40

## List of Tables

1	Comparison of cell width measurements of various stoichiometric fuel-air mixtures at 100 kPa. . . . .	5
2	JP-10 catalytic combustion products . . . . .	24
3	Comparison of cell width measurements of C <sub>6</sub> H <sub>14</sub> -sensitizer-air mixtures with 10 % sensitizer addition (by fuel volume) at 100 kPa. . . . .	42
4	GDT cell width measurements: hexane dilution series. . . . .	48
5	GDT cell width measurements: hexane sensitization series. 'Air'=O <sub>2</sub> +3.76N <sub>2</sub> 49	49
6	GDT cell width measurements: CO mixtures. 'Air'=O <sub>2</sub> +3.76N <sub>2</sub> . (*: cells unreadable) . . . . .	50
7	Composition of HCS mixtures. . . . .	51
8	Hexane vapor phase experiments. Calculated fuel volume: 135 ml. Cell widths are interpolated from experiments performed at initial pressures from 40 kPa to 100 kPa (TableA). .	52
9	Dodecane vapor phase experiments. Calculated fuel volume: 92 ml . . . . .	53



## Part I

# Sensitization of High Molecular Weight Hydrocarbons

## 1 Introduction

Liquid hydrocarbons are the fuel of choice for aviation propulsion systems, including the pulse detonation engine (PDE) concept. Much of the published PDE research carried out up to the present time has used gaseous fuels,  $C_1$ - $C_3$  hydrocarbons, due to the difficulty of creating uniform fuel-air mixtures with liquid hydrocarbon fuels and initiating these mixtures. The present investigation is part of a larger study that considers how liquid fuels can best be utilized in PDEs. This report describes measurements of detonation properties of fuel-blends that are representative of what might be derived by processing liquid hydrocarbon fuels such as JP-10 and Jet-A.

Liquid fuels have obvious storage advantages over gaseous fuels, but tend to be composed of larger, heavier molecules ( $C_6$  to  $C_{12}$ ) and are more difficult to detonate than gaseous fuels such as  $C_1$ - $C_2$ . A liquid hydrocarbon fuel can be partially decomposed into smaller molecules ( $C_1$  to  $C_5$ ) by fuel-rich combustion or by thermal cracking. Fuel-rich catalytic combustion uses the presence of a catalyst to achieve combustion beyond the rich combustion limit, producing reactive molecules, high temperatures and little soot. Catalytic combustion of JP-10 was studied by Brabbs and Merritt (1993) in an effort to find a storable liquid fuel which had an ignition delay time that was less than the residence time in the combustion chamber of a hypersonic vehicle. The majority of the combustion products were low-molecular-weight hydrocarbons that are also more susceptible to detonation, making this process an attractive possibility for PDE fuels.

Smaller molecular weight products may act as ‘sensitizers’ to the parent fuel: reducing the critical energy required to initiate a detonation compared to the parent fuel. The aim of this portion of the study is to investigate the effectiveness of sensitizers on some liquid hydrocarbon fuels by measuring the characteristic cell width of the detonation wave. The cell width is often used to characterize the detonability of a mixture and can be empirically related to parameters such as critical initiation energy, critical diameter or

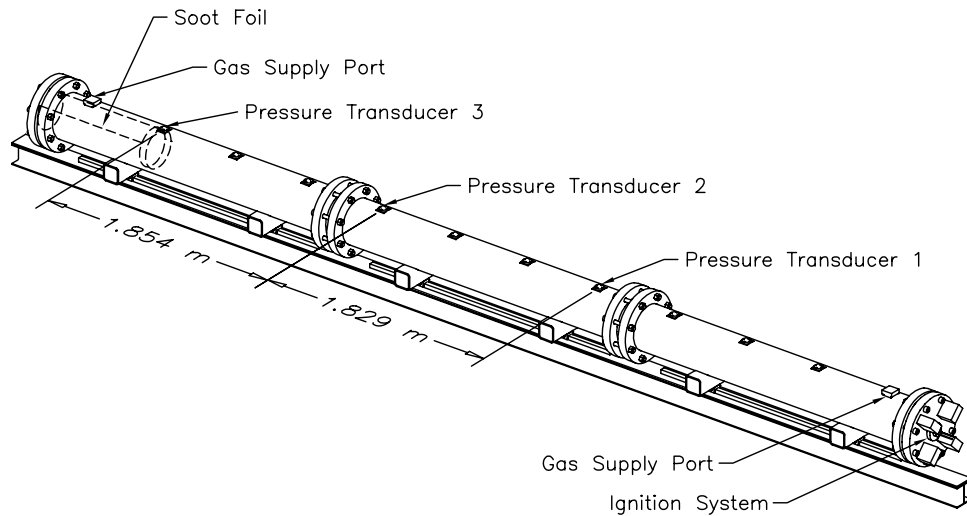


Figure 1: GALCIT 280 mm diameter gaseous detonation facility.

minimum tube diameter. The critical energy required to initiate a detonation is proportional to the cube of the cell width for a spherical source, and directly proportional to the cell width for a planar source (Lee et al. 1982), so fuels which produce smaller cell sizes are more sensitive to detonation. Although direct initiation is not considered feasible for PDE operation, cell width plays an important role in determining if detonations are possible in a given size device. For example, the smallest open area in a tube must be larger than one cell width for deflagration-to-detonation (DDT) to occur. This is an important issue in PDEs which use DDT initiators.

## 2 Facility Description

Detonation cell width experiments were performed in the gaseous detonation tube (GDT) (Akbar 1997, Akbar et al. 1997) shown in Fig.1.

The stainless steel detonation tube is 7.3 m long and has an internal diameter of 280 mm. Before each shot, an aluminum sheet or foil (0.61 m by 0.91 m by 0.5 mm) is rolled, riveted to a steel ring and covered in a light layer of soot. The foil is inserted into the downstream end of the tube and anchored in place. The entire tube is evacuated to about 10 Pa, and then filled by the method of partial pressures. Pressure in the tube is measured by an electronic Heise 901a gauge which is accurate to  $\pm 0.17$  kPa. Hexane

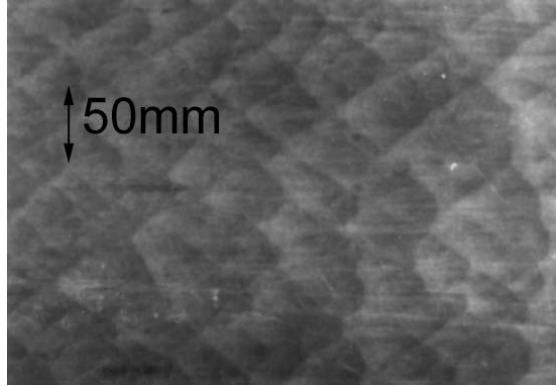


Figure 2: Soot foil for shot 1007:  $C_6H_{14}+9CO+14$  Air. Detonation propagated right to left.

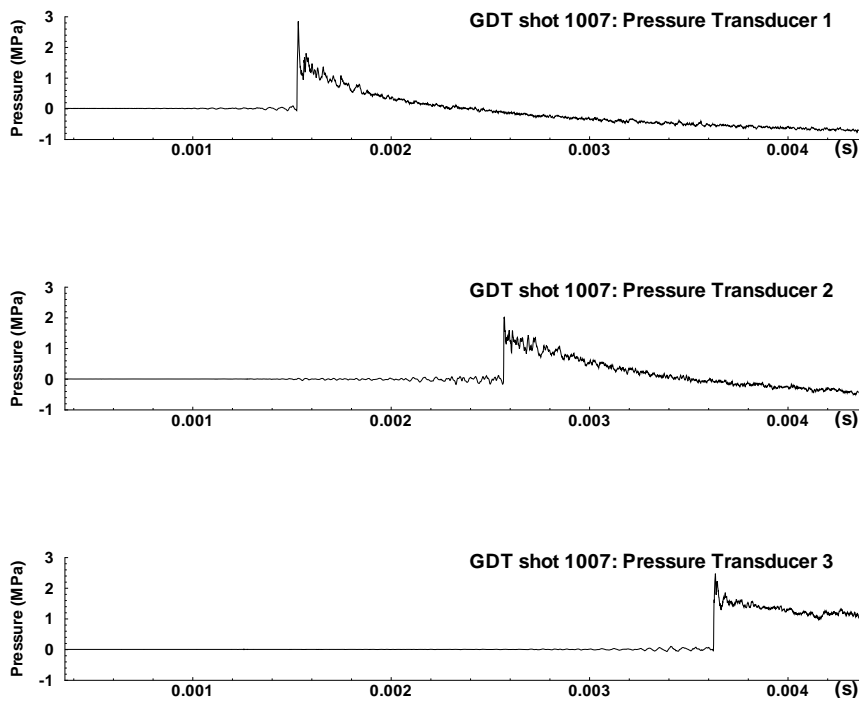


Figure 3: Pressure traces for shot 1007.

is injected into the evacuated tube through a septum. The partial pressure of hexane (vapor pressure of 20 kPa at 298 K) was low enough to ensure that the fuel had vaporized. The partial pressure recorded was at most 0.11 kPa higher than the value calculated based on the liquid volume injected, so this error was within the accuracy of the gauge.

The remaining gases are added to the tube by the method of partial pressures, and the mixture is circulated with a bellows pump for 5 minutes. Ignition is by an exploding wire, created by discharging a 2  $\mu$ F capacitor charged to 9 kV, through a copper wire, initiating an oxy-acetylene driver which is injected just prior to ignition. The equivalent energy of the blast wave transmitted to the test gas is about 70 kJ. Experiments were limited to mixtures producing reflected pressures of 5 MPa, the design limit of the facility. In cases where the reflected pressure of the mixture would exceed 5 MPa, the test was performed at the highest initial pressure possible, then the cell widths for 100 kPa initial pressure were estimated by assuming the cell width varies in inverse proportion to the initial pressure. These data are presented as ‘extrapolated’. All experiments in the GDT were carried out at room temperature, nominally 295 K.

Three PCB pressure transducers, mounted along the tube, record the detonation pressure and time-of-arrival of the wave which is used to calculate a wave speed (Fig. 3). The chemical equilibrium program STANJAN (Reynolds 1986) is used to calculate the Chapman-Jouguet wave speed, pressure, and temperature. The wave speed obtained from the pressure transducers is checked against the calculated value and is typically within  $\pm 1\%$ . The shock triple points in the passing detonation scour a cellular pattern on the soot foil (Fig. 2). There can be quite a range of cell widths recorded for a particular mixture due to the inherent irregularity of the cells. About 10 measurements are made on each foil, and a minimum, a maximum, and an average cell width are recorded. The minimum and maximum give an indication of the range of cell sizes present on a foil. There are also variations in measurement from observer to observer. These can be on the order of  $\pm 50\%$  (Tieszen et al. 1991).

## 3 Cell Width Measurements

### 3.1 C<sub>6</sub>H<sub>14</sub> Mixtures with O<sub>2</sub>-N<sub>2</sub>

The sensitivity of stoichiometric C<sub>6</sub>H<sub>14</sub>-O<sub>2</sub> to nitrogen dilution was investigated. Since the reflected detonation pressure for these mixtures initially at 100 kPa exceeded the facility limit, experiments were performed at 40 kPa or at the highest initial pressure possible in the facility for each mixture. The cell width at an initial pressure of 100 kPa was estimated from these two data points. The average cell width is plotted against  $\beta$  in Fig. 4, where  $\beta$  is the ratio of N<sub>2</sub> to O<sub>2</sub> concentration in the mixture ( $\beta=3.76$  for air). The minimum and maximum cell widths measured are indicated by the error bars. The cell width increased from 1.7 mm at  $\beta = 0$  to 51.1 mm at  $\beta = 3.76$ . Extrapolated cell widths were a factor of 2 smaller than those previously measured at 100 kPa by Beeson et al. (1991).

Fuel	Cell width (mm)	Reference
H <sub>2</sub>	10.9	CIT
CH <sub>4</sub>	280	Moen et al. (1984)
C <sub>2</sub> H <sub>2</sub>	10	Knystautas et al. (1982)
C <sub>2</sub> H <sub>4</sub>	22.8	CIT
C <sub>3</sub> H <sub>8</sub>	51.3	CIT
C <sub>6</sub> H <sub>14</sub>	51.1	CIT

Table 1: Comparison of cell width measurements of various stoichiometric fuel-air mixtures at 100 kPa.

A comparison was made between the hexane and other fuels (Table 1). Cell widths obtained at different  $\beta$  values are shown in Fig. 6 for H<sub>2</sub>, C<sub>2</sub>H<sub>2</sub>, and in Fig. 5 for C<sub>2</sub>H<sub>4</sub>, C<sub>3</sub>H<sub>8</sub>, and CH<sub>4</sub>, all at 295 K and 100 kPa. ‘CIT’ refers to unpublished cell width measurements previously made in the GDT at GALCIT. Hexane cell widths appear to be similar to those of propane, C<sub>3</sub>H<sub>8</sub>. Cell widths for hexane are smaller than those for methane, and larger than those for acetylene or hydrogen. Tieszen et al. (1991) found little variation in cell width with increasing molecular weight for alkanes from ethane to decane, but found differences between hydrocarbons with differing degrees of bond saturation, with alkynes and alkenes producing a smaller cell width than alkanes.

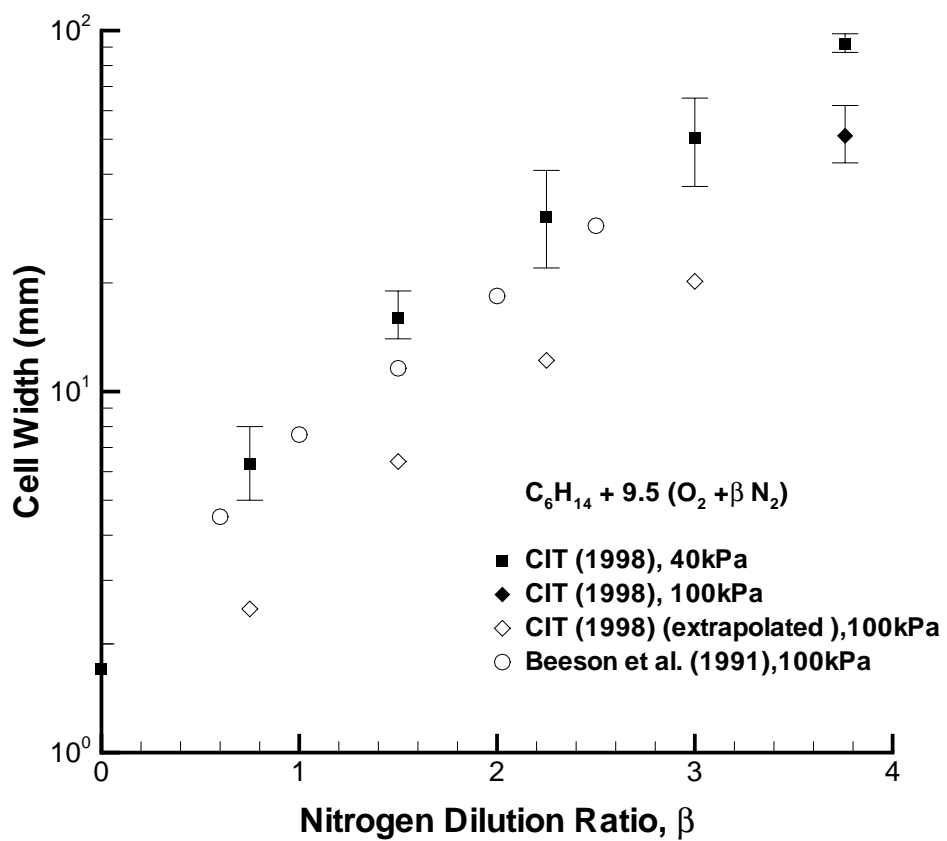


Figure 4: Cell width measurements for  $N_2$  dilution of  $C_6H_{14}-O_2$  mixtures. Experiment parameters are given in Table A

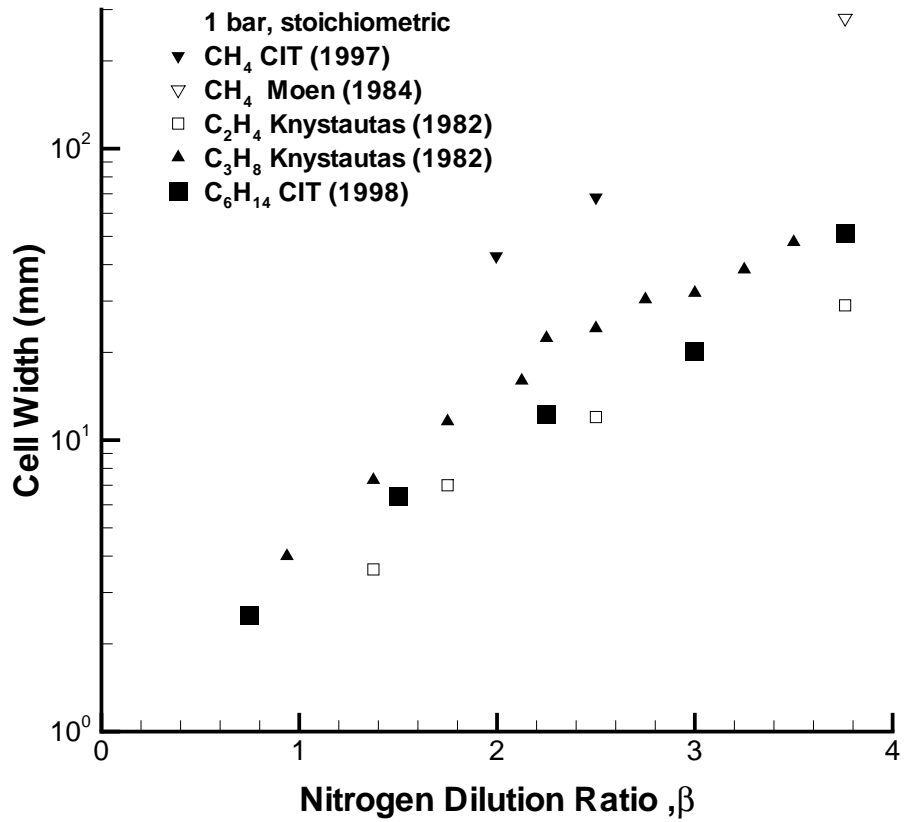


Figure 5: Comparison of cell width measurements for N<sub>2</sub> dilution of CH<sub>4</sub>, C<sub>2</sub>H<sub>4</sub>, C<sub>3</sub>H<sub>8</sub> and C<sub>6</sub>H<sub>14</sub>-O<sub>2</sub> mixtures. C<sub>6</sub>H<sub>14</sub> data is the same as that presented in Fig.4

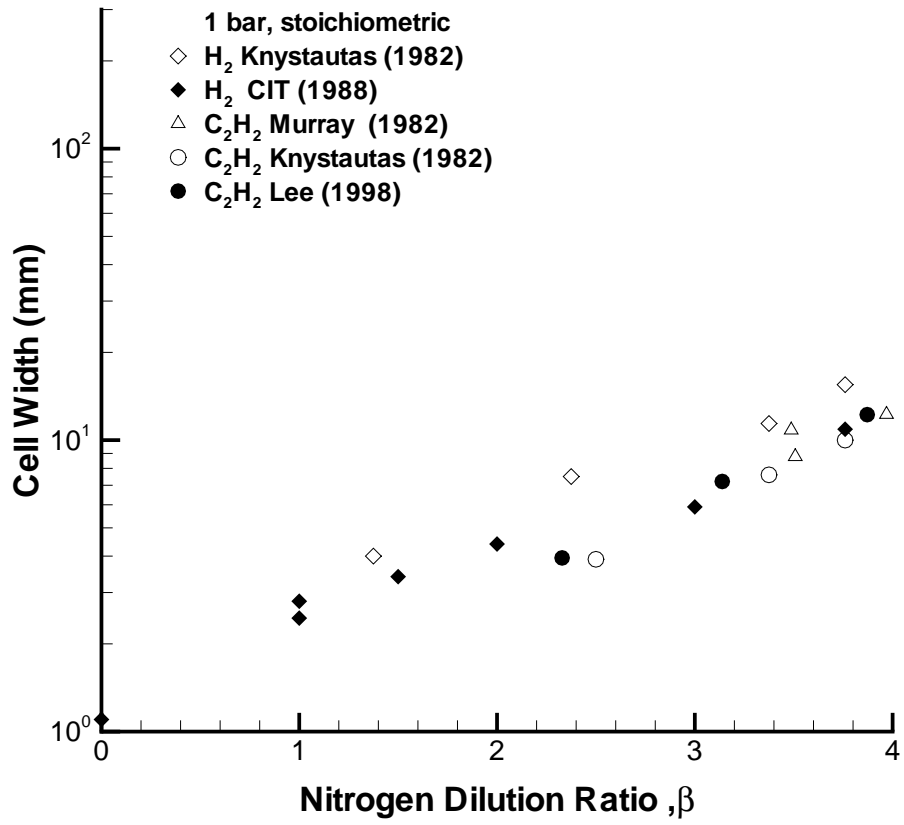


Figure 6: Comparison of cell width measurements for N<sub>2</sub> dilution of H<sub>2</sub>, C<sub>2</sub>H<sub>2</sub> mixtures with O<sub>2</sub>.



### 3.2 Sensitization of C<sub>6</sub>H<sub>14</sub>-air

A series of investigations were made into the sensitizing effects of adding H<sub>2</sub>, C<sub>2</sub>H<sub>2</sub>, C<sub>2</sub>H<sub>4</sub> or CO to C<sub>6</sub>H<sub>14</sub> at 295 K and 100 kPa. The amount of sensitizer was calculated as a mass fraction in the sensitizer-hexane mixture. The appropriate amount of air was added to maintain a stoichiometric mixture. Results are shown in Figs. 7 to 10, with cell width plotted against the percentage (by fuel mass) of sensitizer in the fuel mixture. H<sub>2</sub>, C<sub>2</sub>H<sub>2</sub>, and C<sub>2</sub>H<sub>4</sub> mixtures show a gradual decrease in cell width as the fraction of fuel additive increases; H<sub>2</sub> and C<sub>2</sub>H<sub>2</sub> are more effective than C<sub>2</sub>H<sub>4</sub>. There is no significant variation in cell width for mixtures containing 10 - 70% CO. In mixtures with CO fractions increasing beyond about 75% the cell width increases, indicating the CO acts as an inhibitor. This result is reasonable in view of the subsequent results which confirm the sensitivity of CO mixtures to the presence of hydrogenous species, since the measured cell width increases (indicating reduced sensitivity to detonation) when the initial fraction of H in the mixture is decreased.

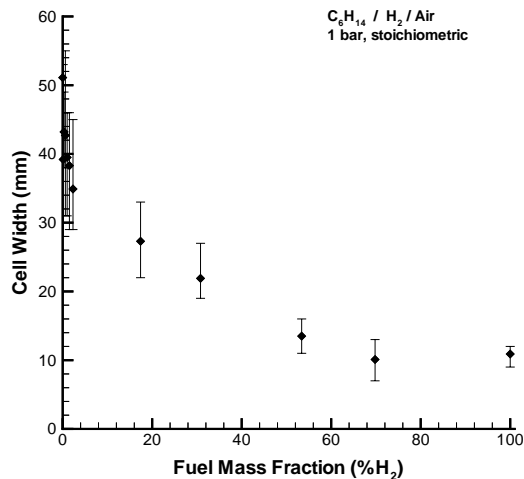


Figure 7: Cell width measurements for H<sub>2</sub> addition to C<sub>6</sub>H<sub>14</sub> in air. Experiment conditions are given in Table A.

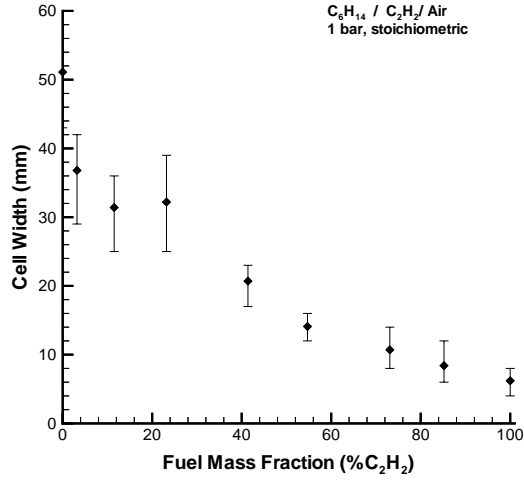


Figure 8: Cell width measurements for  $C_2H_2$  addition to  $C_6H_{14}$  in air. Experiment conditions are given in Table A.

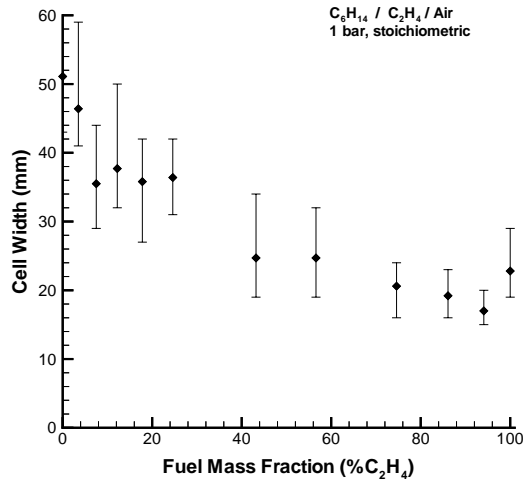


Figure 9: Cell width measurements for  $C_2H_4$  addition to  $C_6H_{14}$  in air. Experiment conditions are given in Table A.

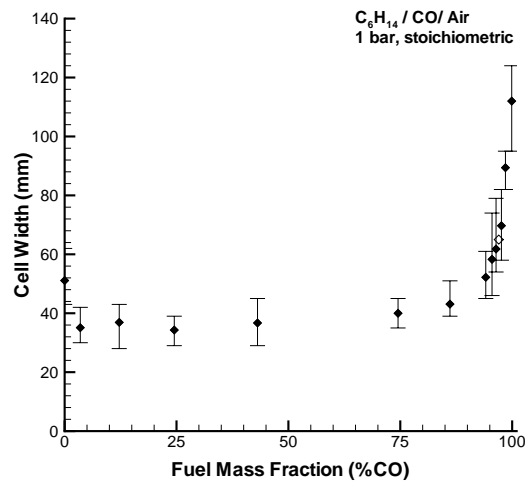


Figure 10: Cell width measurements for CO addition to C<sub>6</sub>H<sub>14</sub> in air. Experiment conditions are given in Table A.

### 3.3 Addition of H<sub>2</sub>, C<sub>2</sub>H<sub>2</sub>, C<sub>2</sub>H<sub>4</sub>, and C<sub>6</sub>H<sub>14</sub> to CO-air

Carbon monoxide is of fundamental importance as a principal intermediate product of hydrocarbon combustion, however there are very little data available on the detonation characteristics of CO. The reaction mechanism is relatively simple and has been studied extensively (Gardiner 1984). In the presence of even trace amounts of hydrogen, the oxidation of CO takes place almost entirely by reaction (1) rather than by the spin-forbidden reaction (2).



Early researchers has found a dramatic increase in the reactivity of carbon monoxide with the addition of water vapor or other substances containing hydrogen (Dixon 1896, Kistiakowsky et al. 1952, White and Moore 1965). The hydroxyl radical promotes oxidation and drastically reduces the induction time. Addition of only 0.02 % H<sub>2</sub> to a CO-air mixture results in a reduction in the calculated reaction zone thickness of three orders of magnitude.

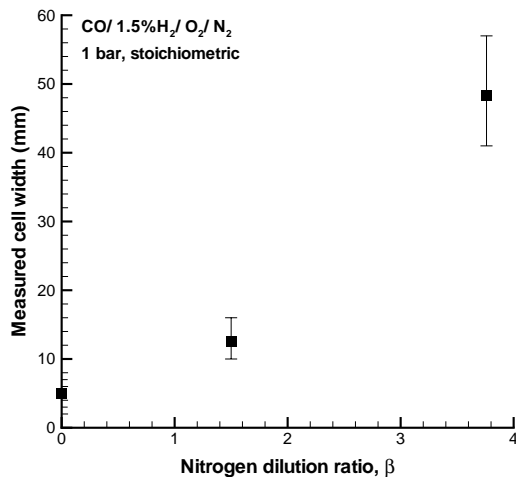


Figure 11: Cell width measurements for N<sub>2</sub> dilution of stoichiometric CO-5% H<sub>2</sub>-O<sub>2</sub>. See Table A for experiment conditions.

The addition of different hydrogenous species to CO-air mixtures was investigated. The fuels  $\text{H}_2$ ,  $\text{C}_2\text{H}_2$ ,  $\text{C}_2\text{H}_4$ , and  $\text{C}_6\text{H}_{14}$  were chosen so as to study the effects of varying atomic hydrogen content and chemical structure. Detonation pressure, velocity and cell width measurements were made. All mixtures were stoichiometric and at 100 kPa and 295 K initial pressure and temperature. Gases used were C.P. grade (99%) and no attempt was made to remove impurities. In these and all other experiments, ‘air’ was formed from 1 part  $\text{O}_2$  with 3.76 parts  $\text{N}_2$ . This avoided using room air which might contain unknown quantities of moisture.

No detonation could be initiated in stoichiometric CO- $\text{O}_2$ . The limiting fraction of  $\text{H}_2$  that was necessary to detonate CO-air was found to be between 0 and 2 % (by fuel volume). Since the mixture CO-2%  $\text{H}_2$ -air resulted in highly irregular cells, a nitrogen dilution series was performed in the mixture CO-5%  $\text{H}_2$  with stoichiometric  $\text{O}_2$  (Fig. 11).

Cell width measurements were made for varying mixture volume fractions of  $\text{H}_2$ ,  $\text{C}_2\text{H}_2$ ,  $\text{C}_2\text{H}_4$  and  $\text{C}_6\text{H}_{14}$  in CO-air (Fig. 12). In all cases, increasing the fraction of additive reduced the cell width. The rate of decrease of cell width is largest with fuel addition of  $\text{H}_2$  and  $\text{C}_2\text{H}_2$ , followed by  $\text{C}_2\text{H}_4$ , then  $\text{C}_6\text{H}_{14}$ . This is consistent with results from Tieszen et al. (1991) who measured cell widths for hydrocarbon-air mixtures and found triply-bonded acetylene had smaller cell widths than doubly-bonded ethylene, which in turn had smaller cell widths than a straight-chain hydrocarbon such as hexane.

A detonation could be initiated in mixtures with only very small fractions of  $\text{C}_6\text{H}_{14}$  (down to 0.07 % of the total mixture). This was the lowest fraction attempted since we were limited by the accuracy of the gauge used during the filling process. In view of the sensitivity of CO oxidation to the presence of hydrogen, this was an interesting result. The hexane molecule contains many more H atoms than the other hydrocarbons considered and so hexane has the highest initial H atom concentration for a mixture at a particular additive concentration. Fig. 13 shows the measured cell width against the initial H atom concentration normalized by the initial CO concentration, where initial H atom concentration is defined as  $n$  times the fuel concentration for the fuel  $\text{C}_m\text{H}_n$ .

To investigate whether the hexane molecule is successful in releasing more H atoms to form OH radicals than an equivalent mixture fraction of the other additives, reaction zone parameters such as species concentrations and temperature were calculated using detailed chemical kinetics mechanisms. Chemical mechanisms were first validated by comparing induction times cal-

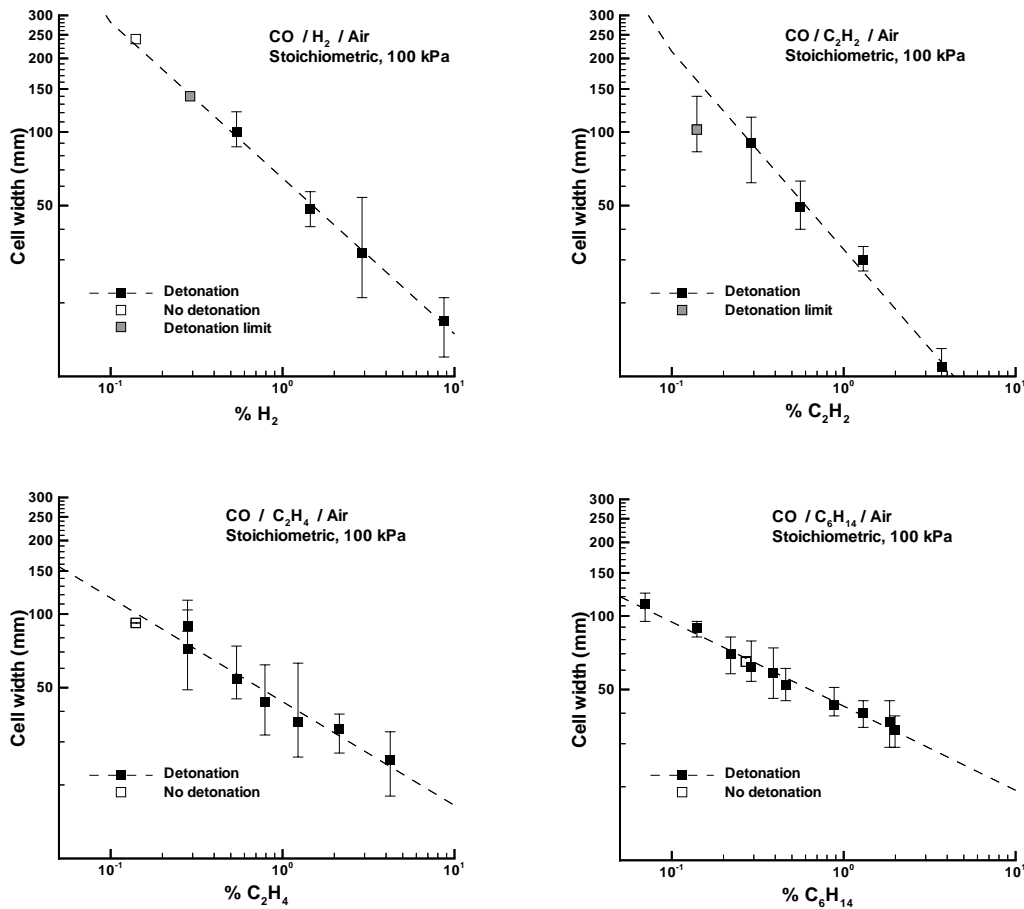


Figure 12: Cell width measurements for hydrogen or hydrocarbon addition to CO-air mixtures. Curves are interpolated from the cell widths of successful detonations. Error bars represent minimum and maximum measured cell widths. The detonation limit denotes a mixture where at least one failure was observed. About three experiments were performed for each mixture that resulted in a failure. Conditions and data are given in Table A

culated with a constant volume explosion assumption with measured shock tube induction times for the same mixtures. Mechanisms were validated against shock tube data for CO-H<sub>2</sub> mixtures and also for mixtures involving the hydrocarbon for which they were considered. The mechanism of War-

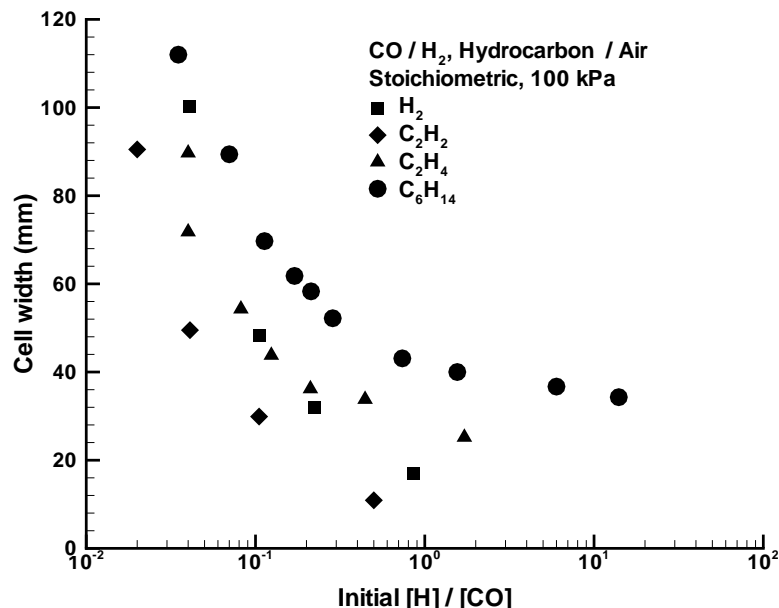


Figure 13: Measured cell width against initial H/CO ratio. Only successful detonations are shown.

natz and Karbach (1997) (34 species, 165 reactions) was chosen for mixtures containing H<sub>2</sub>, C<sub>2</sub>H<sub>2</sub> and C<sub>2</sub>H<sub>4</sub>. The mechanism of Curran et al. (1998) (550 species, 2500 reactions) was used for C<sub>6</sub>H<sub>14</sub> mixtures. Some validations are shown in Fig. 14 and 15. The mechanisms both perform very well against the CO-H<sub>2</sub>-O<sub>2</sub> data of Dean et al. (1978). The largest discrepancy is for the Curran mechanism against the data of Burcat et al. (1996) for which the mechanism underpredicts the experimental results by a factor of 2. Davidson et al. (1999) compared ignition delay times calculated by the Curran mechanism with their shock tube data for heptane mixtures and found the same trends: the mechanism shows a similar temperature dependence as their data but the calculated ignition times are a factor of two shorter than the measured values. A discussion of the range of validity of detailed reaction mechanisms for detonation conditions, possible sources of error in shock tube induction time data and the applicability of a constant-volume calculation for the validation process is given in Schultz and Shepherd (2000).

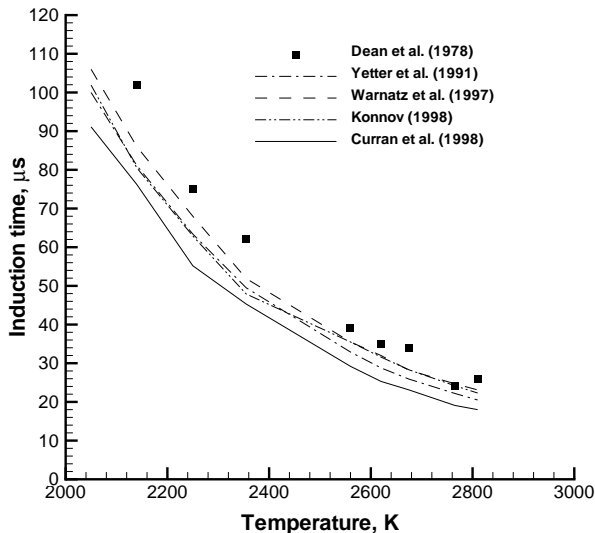


Figure 14: Mechanism validation for CO-H<sub>2</sub>-O<sub>2</sub>-Ar mixtures. Shock tube data is for the mixture 0.049% H<sub>2</sub>, 1.01% O<sub>2</sub>, 3.28% CO, Ar.

A one dimensional Zel'dovich-von Neumann-Doring (ZND) code was used together with the validated mechanisms and CHEMKIN II (Kee et al. 1989) chemical kinetics subroutines to calculate the variation of temperature and species concentrations through the reaction zone. The reaction zone length is typically defined as the distance between the shock and the location of the maximum temperature gradient and can be related to the cell width by a constant of proportionality,  $A$ . This constant has been shown to be different for fuel-O<sub>2</sub> and fuel-air mixtures (Westbrook 1982) and also to vary with the equivalence ratio (Shepherd 1986). In spite of this, both reaction zone length and cell widths decrease with decreasing critical initiation energy and are a useful measure of the sensitivity of a mixture to detonation. Fig. 16 shows measured cell widths against reaction zone lengths. There are some significant deviations from the expected linear relationship. For instance, some of the acetylene mixtures have shorter reaction zone thicknesses due to an early 'bump' (and therefore change in curvature) in the temperature profile. Reaction zone lengths were redefined as the location of the peak in OH mole fraction. The correlation with measured cell width appears more



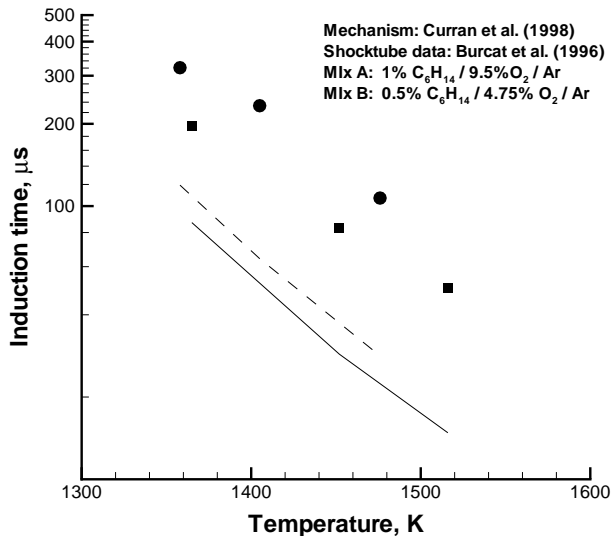


Figure 15: Mechanism validation for C<sub>6</sub>H<sub>14</sub>-O<sub>2</sub>-Ar mixtures. Circles and dashed lines correspond to data and calculations respectively for mixture A. Squares and solid lines correspond to data and calculations respectively for mixture B.

linear (Fig. 16) and this definition of reaction zone thickness will be used for the rest of this section. Values between 25 and 35 were obtained for A.

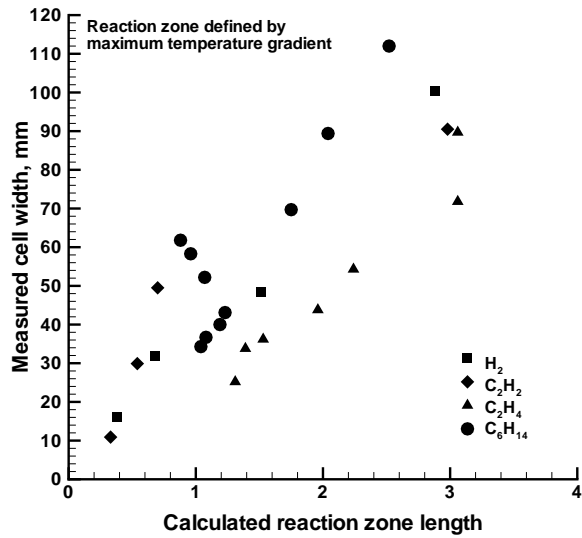
To track the production of the OH radical, species concentrations of CO, CO<sub>2</sub>, OH, O, H and CH were calculated through the reaction zone. As an example, some species concentrations for mixtures with 2% and 30% H<sub>2</sub> (by fuel fraction) are shown in Fig. 17. A large difference in the amount of OH produced by the two mixtures can be seen. The calculated peak OH concentration is shown in Fig. 18 against initial [H]/[CO] ratio. For small initial [H]/[CO] ratio, all mixtures produce about the same peak OH mole fraction. With the addition of more significant fractions of hydrogen or hydrocarbon, the calculated peak OH mole fraction is highest for H<sub>2</sub>, C<sub>2</sub>H<sub>2</sub> and C<sub>2</sub>H<sub>4</sub>. C<sub>6</sub>H<sub>14</sub> produced the smallest peak mole fraction for a given initial [H]/[CO] ratio. A closer look at the species profiles for these C<sub>6</sub>H<sub>14</sub> mixtures shows a peak in the CH and CO mole fraction profiles (Fig. 19). The fall-off in OH production might be attributed to competition between OH and CH

formation reactions.

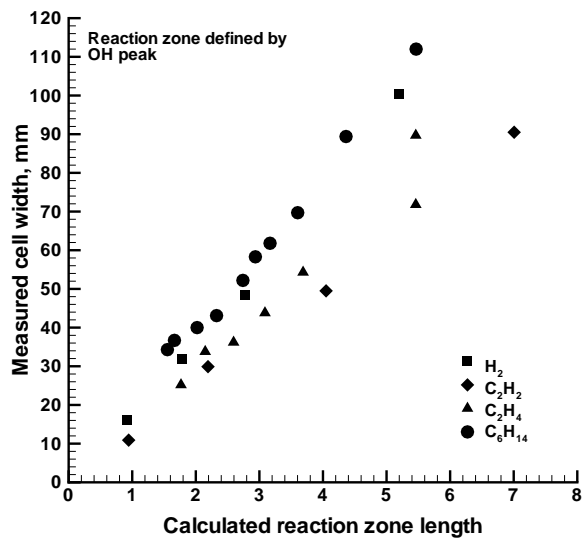
As discussed above, the cell width can be related to the reaction zone thickness by a constant of proportionality,  $A$ . The reaction zone thickness is transformed to an induction time by dividing by the particle post-shock velocity. The induction time,  $\tau$ , may be modeled by identifying a dominant overall reaction for the mixture. A simplified expression for the induction time for a reaction rate with a simple Arrhenius dependence is shown in (3).

$$\tau = \frac{K}{[OH][CO]} \exp \frac{E_A}{RT_s} \quad (3)$$

where  $T_s$  is the post-shock temperature. As the fraction of hydrogen or hydrocarbon added was small, thermal differences between the mixtures considered are small and  $T_s$  is approximately constant, so the temperature term plays a negligible role for these mixtures. Correlating the measured cell width against the inverse of the product of the OH and CO concentrations results in a linear relationship for hydrogen and all the hydrocarbons considered (Fig. 20). The species mole fractions are evaluated at the OH peak. Data for  $H_2$ ,  $C_2H_4$  and  $C_6H_{14}$  collapses onto a single curve while the  $C_2H_2$  mixtures obey the similar linear relationship but the data fall a factor of two below that of the other additives. This relationship between the cell size and the OH and CO concentrations suggests that reaction (1) is in fact a dominant reaction for CO mixtures in the presence of hydrogenous species.



a)



b)

Figure 16: Cell width measurements versus reaction zone thickness in CO-O<sub>2</sub> mixtures with hydrogenous additive at 100 kPa. The reaction zone thickness is defined by a) the location of the maximum temperature gradient or b) by the location of the OH peak.

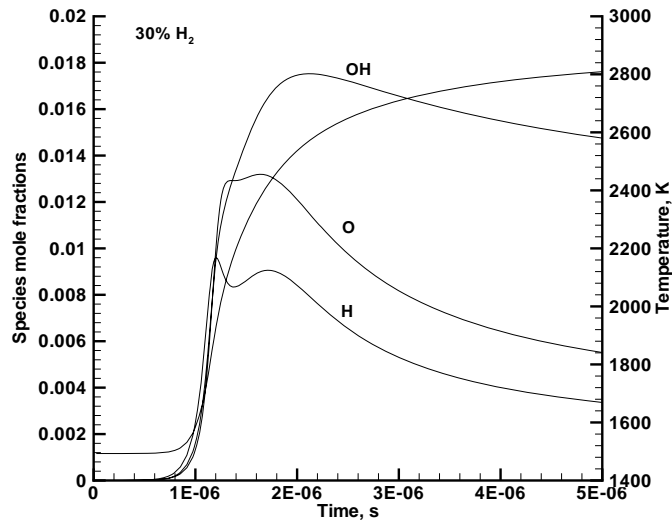
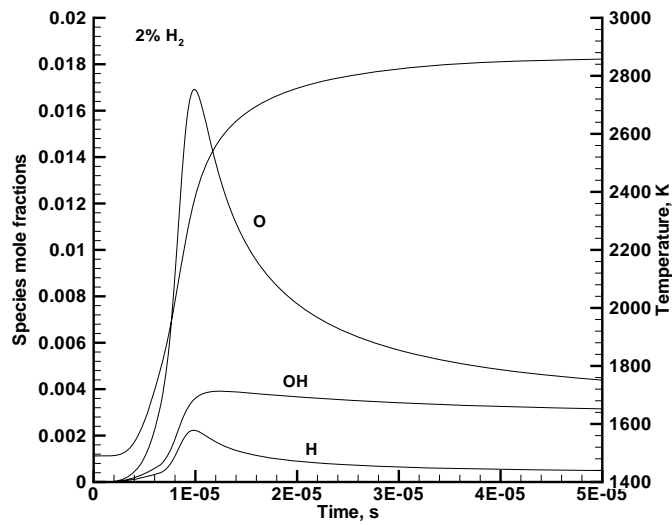


Figure 17: Calculated species mole fractions through the reaction zone in stoichiometric CO-H<sub>2</sub>-air mixtures. H<sub>2</sub> quantities are by fuel mole fraction.

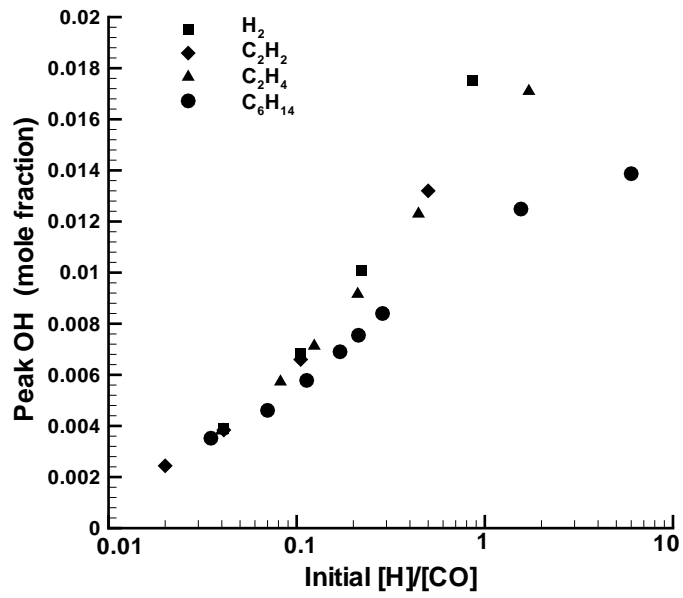


Figure 18: Peak OH mole fraction against initial [H]/[CO] ratio.

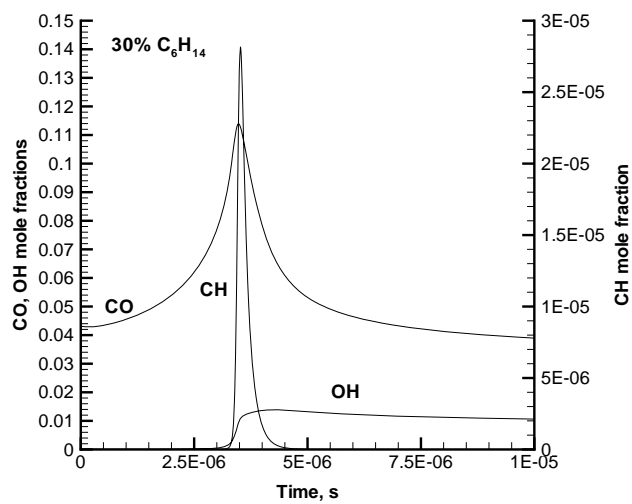
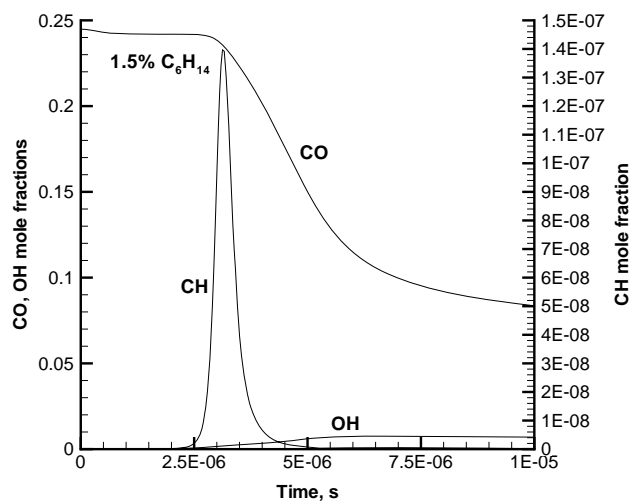


Figure 19: Calculated species mole fractions through the reaction zone in stoichiometric CO- $C_6H_{14}$ -air. Note the differences in scale on the ordinate axis.

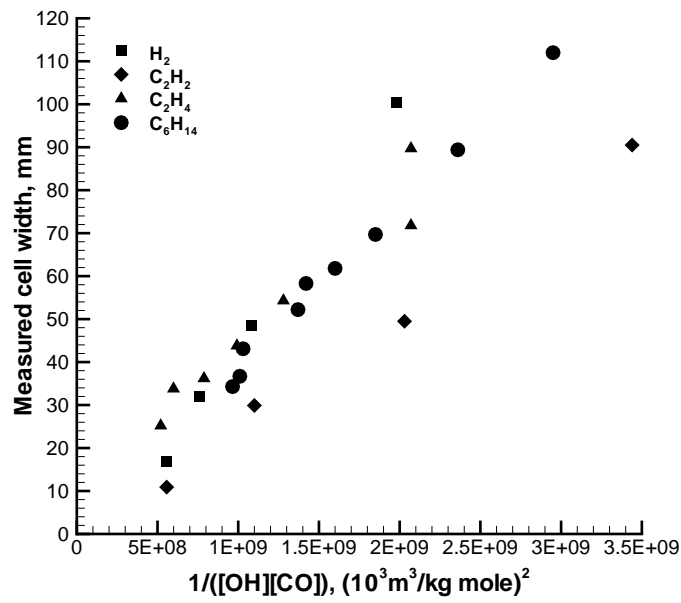


Figure 20: Correlation of measured cell width against the parameter  $1/([\text{OH}][\text{CO}])$ . Species concentrations are calculated by a ZND code and evaluated at the OH peak.

### 3.4 Decomposed JP-10 Surrogate (HCS)

Brabbs and Merritt (1993) investigated the fuel-rich catalytic combustion of JP-10 for a range of equivalence ratios. We have used their results to create a mixture similar to the decomposition products and tested this mixture in our detonation tube. The mixture chosen for this study (Table 2) resulted from JP-10 combustion at an equivalence ratio of 5.06, with a reaction temperature of 1220 K. Group 2 hydrocarbons are those with 3 or more carbon atoms. The remaining fraction consisted of condensible products which were not analyzed.

CO <sub>2</sub>	H <sub>2</sub>	CO	CH <sub>4</sub>	C <sub>2</sub> H <sub>2</sub>	C <sub>2</sub> H <sub>4</sub>	Group 2	O <sub>2</sub>	N <sub>2</sub>
3.37	8.07	14.70	2.88	0.73	4.24	3.03	1.38	60.79

Table 2: JP-10 catalytic combustion products

A hydrocarbon surrogate (HCS) blend was made by omitting the O<sub>2</sub>, N<sub>2</sub> and CO<sub>2</sub> from the mixture given in Table 2. Hexane was chosen as a representative larger hydrocarbon from Group 2. Four of the components of the blend (H<sub>2</sub>, CO, CH<sub>4</sub>, and C<sub>2</sub>H<sub>4</sub>) were premixed by the manufacturer to an accuracy of  $\pm 2\%$  on each component. This was done to improve the repeatability of the tests.

The HCS blend was mixed with a stoichiometric amount of O<sub>2</sub> and diluted with N<sub>2</sub> (Table 7). Experiments were performed at 295 K and at the maximum pressure possible in the facility. The pressure was limited by the design strength of the tube. Cell widths were obtained for several  $\beta$  values (Fig. 21), and decrease from 27.6 mm for  $\beta = 3.76$  (i.e. fuel blend-air) to 1.0 mm for  $\beta = 0$  (i.e. fuel blend-oxygen), a decrease in the spherical critical initiation energy of four orders of magnitude.

The mixture for shot 1067 is the HCS blend together with the O<sub>2</sub> and N<sub>2</sub> remaining after the catalytic combustion. Sufficient air was added so that the mixture was stoichiometric. Since most of the original oxygen had been consumed in the combustion of JP-10, this resulted in a  $\beta$  ratio greater than that of air. The cell width for this case was 55.8 mm which is very close to the 51.1 mm cell width measured for C<sub>6</sub>H<sub>14</sub>-air (Section 3.1). If the HCS blend is mixed with stoichiometric O<sub>2</sub> and no N<sub>2</sub> is added beyond that which would result from the catalytic combustion,  $\beta = 1$  and the extrapolated cell width at 100 kPa is about 4 mm. Thus we estimate the spherical critical



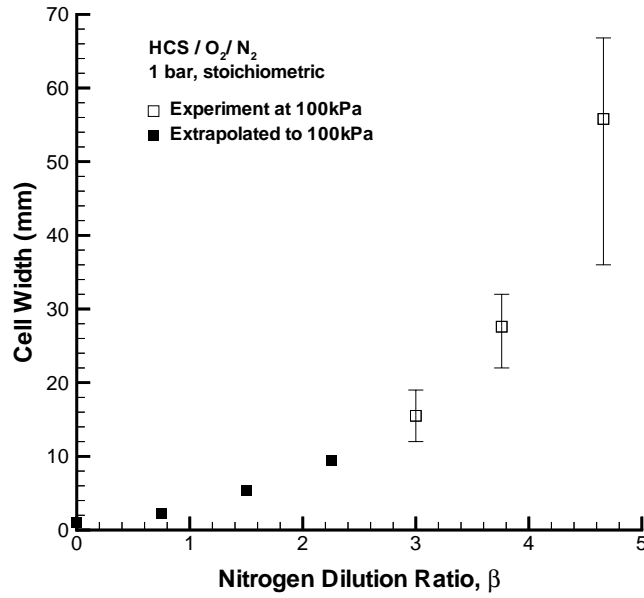


Figure 21: Cell width measurements for N<sub>2</sub> dilution of a hydrocarbon blend representative of decomposed JP-10. The initial pressure was increased with increasing N<sub>2</sub> dilution.

initiation energy can be reduced by three orders of magnitude if the combustion products of JP-10 catalytic combustion are detonated in oxygen rather than in air.

## Part II

# Homogeneous and Heterogeneous Detonations in $C_6H_{14}$ and $C_{12}H_{26}$

## 4 Introduction

Liquid hydrocarbon fuels can be pre-heated to vapor phase, or alternatively, injected into a combustion chamber in a fine spray. Papavassiliou et al. (1992) initiated detonations in decane sprays of  $5\mu\text{m}$  and found the cell size increased by a factor of two over cell sizes obtained for vapor phase detonations at  $100\text{ }^\circ\text{C}$ . They report a cell width of 4 mm for decane spray-oxygen detonations at an equivalence ratio of about 0.95.

In this study, a jet-initiation facility was used to try to detonate both vapor phase and droplet phase mixtures of a representative heavy hydrocarbon (dodecane). Cell width measurements are not available for dodecane, so the critical nitrogen dilution limit was used as a measure of the detonability. Vapor phase dodecane experiments were performed at 380 K. Detonations were initiated in vapor phase hexane mixtures for comparison.

## 5 Facility Description

Experiments were performed in the HYJET facility (Fig. 22). A brief facility description is given below, for more details see Krok (1997). The facility consists of two vessels, a driver and a receiver chamber, initially separated by a Mylar diaphragm. The driver has a volume of  $0.028\text{ m}^3$  and an inner diameter of about 114 mm, although there are variations in cross-sectional area along its length. Interchangeable nozzles mate to the end of the driver and retain the diaphragm. Only the 92 mm diameter nozzle was used in these experiments. The driver extends into the receiver, which has a volume of  $1.19\text{ m}^3$  and an outer diameter of 0.91 m.

The receiver can be heated to a maximum gas temperature of 383 K and was maintained at 380 K for the vapor-phase dodecane experiments. The

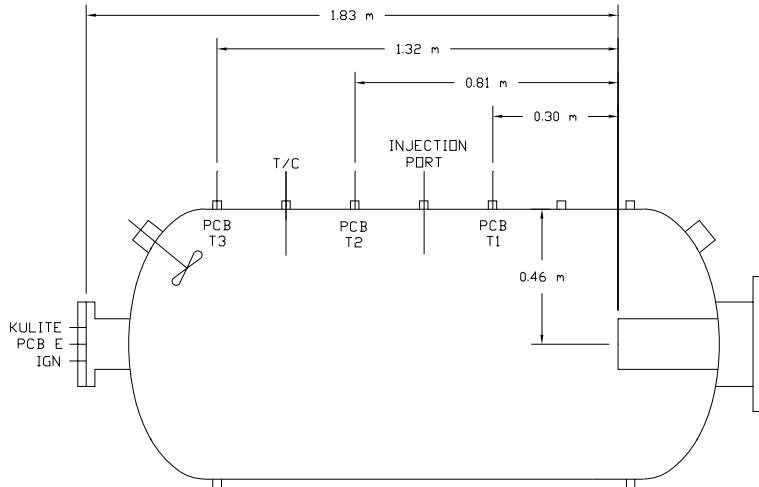


Figure 22: HYJET receiver instrumentation. (Driver vessel not shown.)

vessel walls are heated by condensing steam inside the vessel and by electrical heating pads and tapes. The temperature is monitored by a thermocouple gauge positioned in the receiver vessel.

Both vessels are evacuated to less than 40 Pa, then filled by the method of partial pressures. The liquid fuel is injected through a septum. Sufficient fuel was injected to achieve the required partial pressure; the volume of hexane injected varied between 1 and 1.3 times the calculated volume and the dodecane required 1.1 and 1.6 times the calculated amount. There was no obvious correlation between the volume required and the other test parameters (see Appendix A). A similar effect was observed by Tieszen et al. (1991) when vaporizing liquid hydrocarbon fuels up to decane. The amount of liquid fuel required was 1.25 - 2 times the amount calculated, with the error increasing as the molecular weight of the fuel was increased. It was determined the soot in the facility absorbed fuel from the gas phase. It is expected that a similar effect occurs in the HYJET facility.

The driver mixture is initiated by a 30 kV spark. More detailed driver characteristics are given below. A thermocouple and three PCB transducers (T1,T2,T3) are located along the receiver and a fourth PCB is located on the end flange as shown in Fig. 2.1. These PCB transducers record the pressure

and time-of-arrival of the detonation wave. The trigger for the driver spark also triggers the data acquisition. The driver flange is instrumented with two pressure gauges (a PCB and a Kulite) and thermocouple gauge.

## 6 Driver Characterization

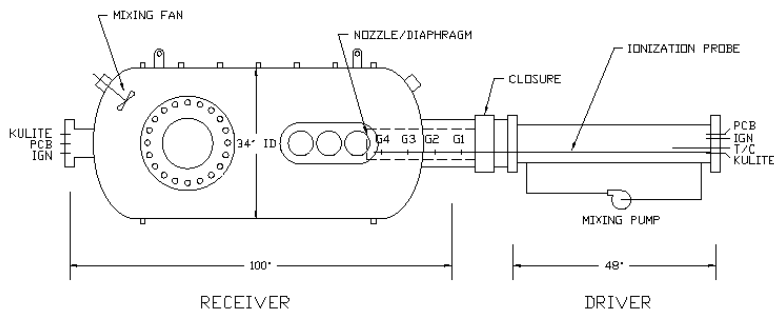


Figure 23: Ionization gauge located in the driver of the HYJET facility. The receiver contained air at 1 atm.

The driver mixture was 60%  $H_2$ , 15%  $O_2$ , 25%  $N_2$  at an initial pressure of 1.114 bar. The same driver was used throughout this series of experiments. Various  $H_2$ ,  $O_2$ ,  $N_2$  driver compositions had been previously investigated (Krok 1997), by determining the lean limit of detonation initiation in the receiver. For receiver mixtures that were 0-30%  $H_2$  in air at 1 atm, it was determined that the above driver was most effective, as it was able to give prompt initiation with only 24%  $H_2$  in the receiver mixture, a  $D/\lambda$  ratio of 4.3, where  $D$  is the diameter of the jet and  $\lambda$  is the detonation cell size of the mixture. A driver with no  $N_2$  dilution required the receiver mixture to contain more than 26%  $H_2$  before it could be detonated.

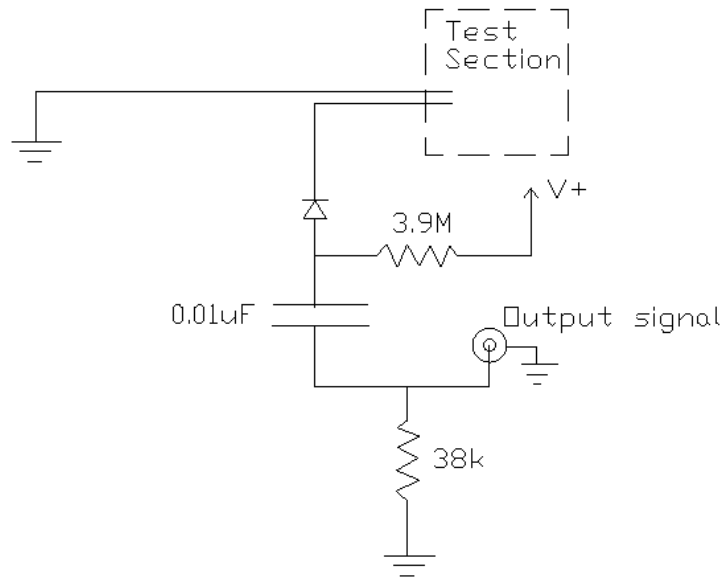


Figure 24: Schematic of the ionization gauge circuit,  $V^+=12V$ .

Krok's results indicated the 60%  $H_2$ , 15%  $O_2$ , 25%  $N_2$  driver may be transitioning to detonation, but there wasn't sufficient instrumentation in the facility to be sure. To characterize the driver more thoroughly, an ionization probe has been built consisting of four gauges (G1, G2, G3, G4) mounted on a sting extending from the back flange of the driver (Fig. 23). The gauges are 178 mm apart and G4 is positioned 100 mm upstream of the diaphragm location. The gauges are all positioned in the part of the driver that is of uniform cross-sectional area. A schematic of the ionization gauge circuit is shown in Fig. 24. Time-of-arrival data and wave speeds (Fig. 25) show that the driver does indeed transition to detonation, and at 100 mm from the diaphragm it is probably an overdriven detonation as the CJ velocity of the driver mixture is calculated to be 2571 m/s. The receiver mixture was air at 1 atm.

A subsequent study (Pfahl and Shepherd 1999) determined the critical  $N_2$  dilution limit for  $H_2$ - $O_2$  mixtures in the receiver of the same facility using a driver that didn't transition to detonation before the nozzle exit. Pfahl and Shepherd (1999) found  $8 \leq D/\lambda \leq 11$  which, as expected, is higher than the ratio of around 4 determined for the detonating driver. Results for other flame-jet drivers also show higher  $D/\lambda$  ratios: Carnasciali et al. (1991)

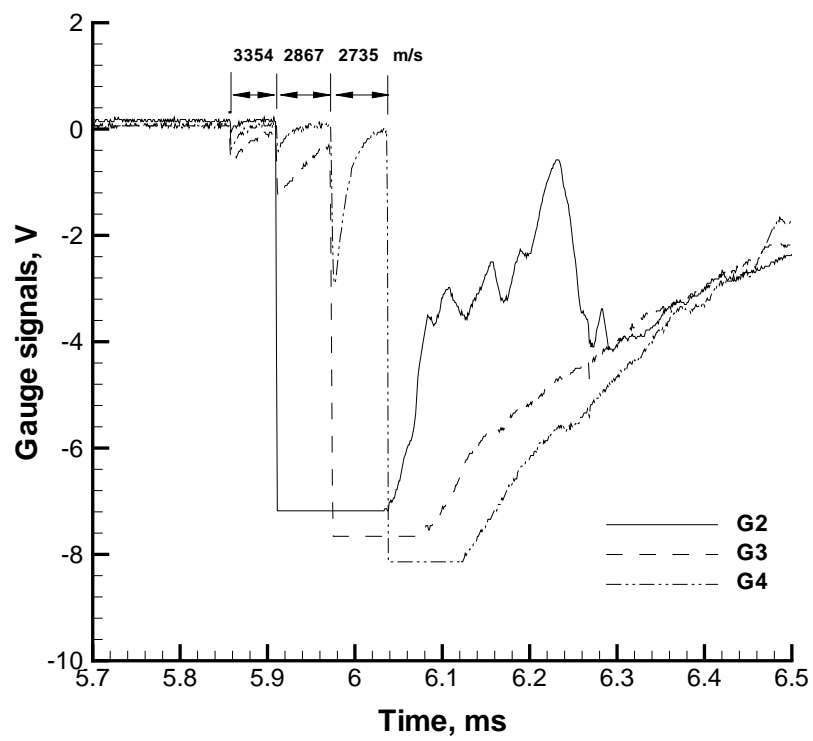


Figure 25: Time-of-arrival data from ionization gauges in the driver.

obtained  $8 \leq D/\lambda \leq 15$ , Bezmelnitsin et al. (1997) obtained  $18.5 \leq D/\lambda \leq 24$ .

The initial pressure for  $N_2$ -diluted drivers had been increased over 1 atm in an attempt to compensate for the reduced peak driver pressure. However, the peak pressures recorded in the driver were found to be higher than expected (Krok 1997). This was attributed to a dynamic effect of the confinement geometry, which is not considered by the equilibrium code used to predict the  $P_{AICC}$  pressure.

## 7 Vapor Phase Experiments in Hexane and Dodecane

### 7.1 Hexane

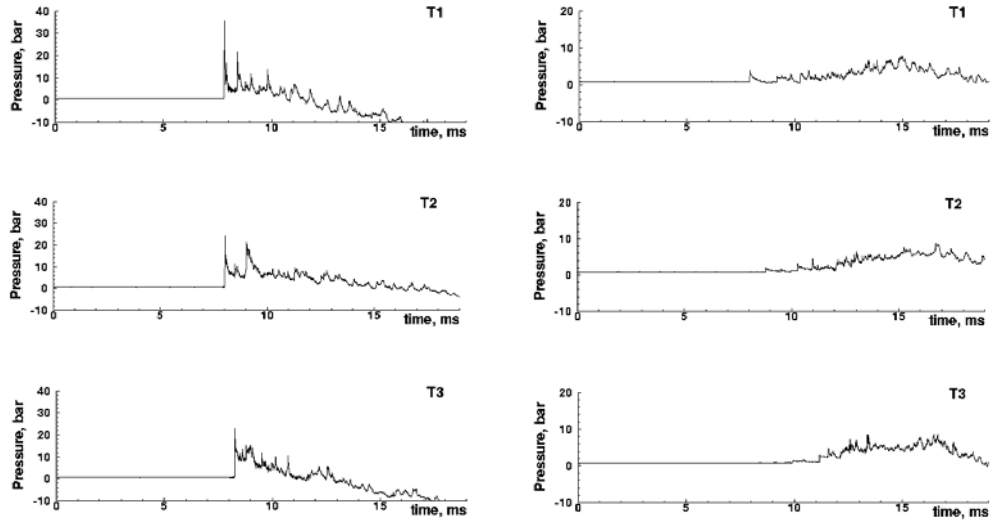


Figure 26: Pressure traces recorded along the receiver vessel wall for vapor phase  $C_6H_{14}$ - $O_2$ - $N_2$  mixtures. On the left,  $\beta = 2.25$  (shot 569). The initial pressure was 690 mbar, the initial temperature 298 K. On the right,  $\beta = 3.0$  (shot 571). The initial pressure was 844 mbar, the initial temperature 296 K. Note the difference in scale on the ordinate axes.

The critical nitrogen dilution limit, defined as the maximum value of  $\beta$

for a mixture that can still be detonated in this facility, was determined for stoichiometric mixtures of  $C_6H_{14}-O_2$ . To keep within the maximum design pressure of the facility, the partial pressures of  $C_6H_{14}$  and  $O_2$  were kept constant for each shot. The total pressure then depended on the amount of nitrogen added. A detailed description of the conditions for each test is given in Appendix A. The vapor pressure of  $C_6H_{14}$  is high enough that the facility did not need to be heated for this series. Pressure traces are shown in Fig. 26 for two values of  $\beta$ , where  $\beta$  is the ratio of nitrogen to oxygen concentration in the mixture.

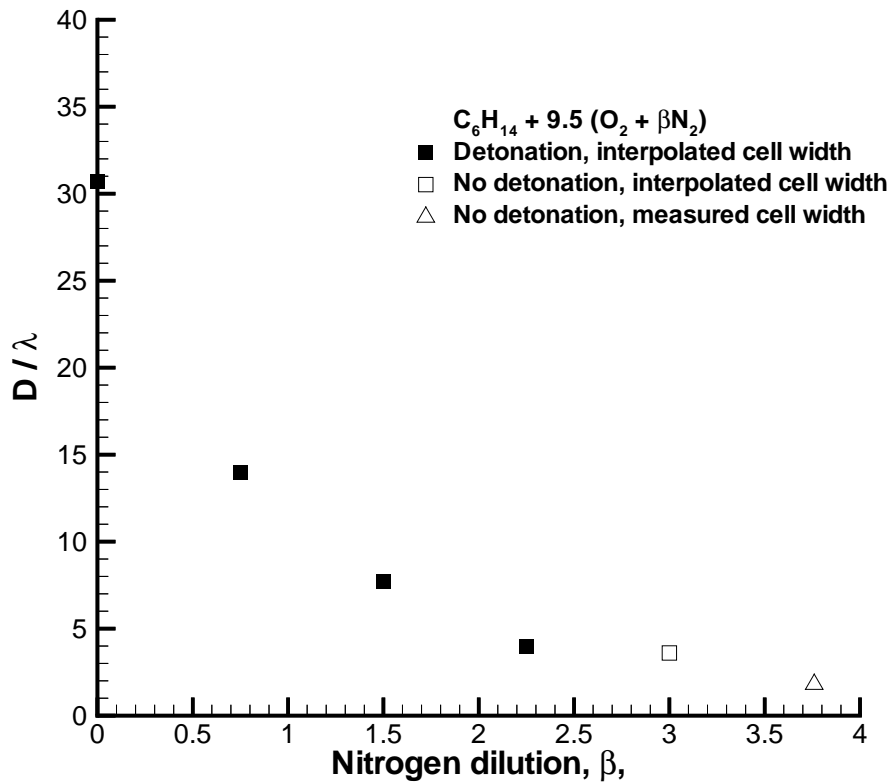


Figure 27:  $D/\lambda$  (nozzle diameter/measured cell width) variation with nitrogen dilution. Initial pressure increased with increasing  $N_2$  dilution.

The equilibrium code STANJAN (Reynolds 1986) was used to calculate



CJ pressure, reflected pressure, and CJ velocity for each test. These calculated values, together with measurements, are given in Appendix A. Direct initiation was observed up to  $\beta = 2.5$ . For these cases, the peak pressure at the first transducer location (T1) is usually comparable to the calculated reflected wave pressure (around  $2.5P_{CJ}$ ). The pressure decays as the wave passes from T1 to T3, but remains above  $P_{CJ}$ . The wave speed, obtained from the time of arrival at the three locations (T1,T2,T3), is up to 37% higher than the calculated CJ value, and decreases as the wave propagates from T1 to T3. Although the variation in the volume of liquid fuel injected was not systematic, the CJ wave speed corresponding to a mixture with the actual volume of fuel injected was also calculated and found to be about 5% higher than the stoichiometric value, so the excess liquid fuel injected (which is presumed to have been absorbed by the soot in the vessel) can not account for the high wave speed observed in experiments.

If the detonation in the receiver mixture is initiated near the jet exit, it will expand like an unconfined spherical detonation. The detonation wave will be curved rather than planar and will not propagate parallel to the wall but at an oblique angle. When the wave reaches T1 it may still have significant curvature so that the pressure recorded is close to the reflected pressure. The wave will flatten out as it propagates down the vessel decreasing the angle of incidence between the wave and the wall. For angle of incidence greater than about  $60^\circ$ , a Mach reflection will occur. This will affect the interpretation of the pressure measurements. It is also possible that the reactants are driven downstream by the jet flow and the detonation is initiated only after sufficient time for entrainment and an ignition delay period (see (Krok 1997)). In this case, the time-of-arrival at the three pressure transducers would be similar and a high wave speed would be inferred.

No detonation was directly initiated at  $\beta \geq 3.0$  (Fig.26) although a delayed secondary explosion was observed. The peak pressures following the shock (0.4-0.2 MPa) and the wave speeds (around 500 m/s) were substantially less than the CJ values ( $P_{CJ}=1.72$  MPa,  $U_{CJ}$  1853 m/s). Cell width measurements made in the GDT facility for hexane were interpolated to match the pressure of the HYJET data (Appendix A). The critical  $D/\lambda$  ratio is about 4 (Fig. 27) and compares well with a previously determined value of 4.3 for this driver .

## 7.2 Dodecane

A similar nitrogen dilution series was performed in stoichiometric  $C_{12}H_{26}-O_2$ . Again, the partial pressures of  $C_{12}H_{26}$  and  $O_2$  were kept constant to keep the reflected pressure within facility design strength limits. The facility was heated to maintain a gas temperature of about 380 K, although variations of  $\pm 1$  degree did occur during the filling process. Measured and calculated properties for each test are given in Appendix A. A detonation could be directly initiated up to  $\beta=2.5$  (Fig. 28). Both the wave speed and peak pressure were higher than the calculated CJ condition, but decayed as the wave propagated in the receiver. No detonation was directly initiated at  $\beta = 3.0$  resulting in a critical  $N_2$  dilution limit similar to hexane. No DDT regime was observed although a secondary explosion was observed in  $\beta = 3.0$  mixtures after sufficient time had passed for shock reflection and shock focussing to precondition the mixture.

